RESEARCH ARTICLE

An Open-Source Fast Integral Transform Program for Quantum-Mechanical Wavefunction Propagation and Corresponding Eigenvalue and Eigenfunction Determination in one Spatial Dimension

Christopher J. Sweeney[1,*]

[1] Northwest Florida State College, Niceville, Florida 32578-1347, United States

Abstract

The underpinnings, usage, and capabilities of source code developed to simultaneously compute and display the temporal evolution of quantum-mechanical wavefunctions are described. This computation is done through direct numerical integration of Schrödinger's equation and is limited to one spatial dimension. The source code is freely downloadable for noncommercial, educational purposes. The Schrödinger equation's linearity in facilitating the computations along with important restrictions imposed by the algorithms employed are emphasized. Physical interpretations of the example systems treated are highlighted. Plenty of citations and footnotes are provided—both historical and pedagogical. The hope is that the source code will be valuable to both students and faculty involved with advanced undergraduate and beginning graduate quantum mechanics and quantum chemistry courses, and will be modified and used for their own projects.

Submitted: 02 April 2026
Accepted: 22 April 2026
Published: 27 May 2026

Vol. 2, **No.** 1, 2026.
10.62762/JNSPM.2026.747031

***Corresponding author:**
✉ Christopher J. Sweeney
sweeneyc@nwfsc.edu

Keywords: Approximate solution of partial differential equations, Solution of Schrödinger's equation numerically using fast integral transforms, Visualization of wavefunction evolution in quantum mechanics and quantum chemistry.

1 Introduction

Since its inception just about a century ago, quantum mechanics has given the best available description of the structure and dynamics of pieces of matter around the size of atoms or smaller. Quantum mechanics can be mathematically formulated in a variety of ways—through matrices, [1–3] by employing abstract Hilbert spaces, [4, 5] with path integrals, [6, 7] or by using wavefunctions. [8–13]

But most people prefer the wavefunction approach over the others, chiefly because it's intuitive and visual. The visual nature of wavefunctions is especially good at highlighting notions like interference, superposition states, and Heisenberg's uncertainty principle—notions missing from the erroneous description of atomic and smaller-sized particles that classical mechanics gives [14].

Citation
Sweeney, C. J. (2026). An Open-Source Fast Integral Transform Program for Quantum-Mechanical Wavefunction Propagation and Corresponding Eigenvalue and Eigenfunction Determination in one Spatial Dimension. *Journal of Numerical Simulations in Physics and Mathematics*, 2(1), 39–58.

Wavefunctions are often used to study atomic, molecular, and nuclear collisions. Such collisions are important because they underlie all chemical and non-relativistic nuclear reactions [15, 16]. Customarily the wavefunctions employed here are stationary ones—solutions to the time-independent *part* of Schrödinger's equation. To treat these collisions we choose wavefunctions describing the particles long before they collide. Next we solve this part of Schrödinger's equation for the potential-energy function (or "potential") describing how the involved particles interact when they hit each other. We then examine the character of the resulting wavefunctions far from where the particles hit. Such character indicates what the particles are doing long after the collision is over. Finally we map the "before collision" and "after collision" wavefunctions to each other with quantities called scattering (or "S-") matrices.

Experiments to measure what's going on when atomic and subatomic particles hit together typically start out with collimated, monoenergetic beams of the particles we're interested in, and then collide these beams together. Particles resulting from the collisions—which might not be the same kinds as the ones we began with—are picked up by detectors usually placed far away from where the original particles smashed together. The results of these experiments are most often reported as quantities called "cross sections." They get this name because they have the dimensions of area, and they amount to the likelihoods of various processes happening during collisions [17].

A cross section might spell out, for example, the chance of a neutron bouncing off the nucleus of a silver atom and pumping that nucleus into an excited state. A cross section could also indicate the possibility of an electron colliding with a helium atom while leaving this atom in the same state that it started in. Cross sections can even be used to quantify the likelihood of really complicated processes happening—like a hydrogen atom hitting a deuterium fluoride molecule making a deuterium atom and a hydrogen fluoride molecule afterwards.

When theoretically-predicted S-matrices and experimentally-measured cross sections match up we gain confidence that we understand the collisions' outcomes pretty well [18]. But S-matrices and cross sections leave a lot to the imagination about what goes on during collisions. Just like a story written in a book, a collision has a beginning, a middle—where the action happens—and an end. The most intuitive way to understand what's happening during the middle of a collision's story is to picture how the wavefunction describing it changes while the colliding particles are hitting each other.

In this article we report on source code we've developed to do just this. Our source code computes the temporal evolution of wavefunctions for collisions that can be represented in one spatial dimension, and displays the evolving wavefunctions as "movies" on a computer screen while the calculations are being performed. If bound states are supported by the collision system, then the software can be used to find their corresponding eigenenergies and position-space eigenfunctions. Our source code can be freely downloaded as a companion to this article from https://github.com/cjssjccjs/qmechonedim/ for educational and noncommercial purposes, and can easily be modified to handle essentially any one-dimensional system—so long as a potential for it can be expressed as a mathematical function.

We begin by detailing the method we used for solving Schrödinger's equation in an arbitrary number of spatial dimensions since even though we're treating just one spatial dimension here, the method can be generalized to as many spatial dimensions as we want. After this, we cover the advantages and limitations of the numerical algorithms used—but here only in one spatial dimension because it's easier to understand them this way. To demonstrate our software's accuracy and efficiency we then present a comparison of our results to some well-known previous ones for rectangular barriers and wells. Next we handle a situation described by a more realistic potential—one commonly used to characterize the vibrations of nuclei in diatomic molecules.

Throughout our treatment we emphasize the mathematical, numerical, and physical insights salient in our approach. Plenty of footnotes along with extensive citations are provided to support what we cover here for those who want to modify and extend it for their own projects. We hope that the software will be helpful to both students in advanced undergraduate and beginning graduate quantum mechanics and quantum chemistry courses and to the faculty who teach them.

2 Theoretical and Numerical Approach

To start we need a way to propagate a system's wavefunction $\Psi(\mathbf{r}, t)$ through a collision by solution of Schrödinger's equation. With $\mathbf{r}$ the vector representing the system's spatial position and t the time, this

equation says that

$$\mathbf{H}\Psi(\mathbf{r},t) = i\hbar\frac{\partial}{\partial t}\Psi(\mathbf{r},t). \quad (1)$$

Here $\mathbf{H} = \mathbf{T}+\mathbf{V}$ is the Hamiltonian operator, where $\mathbf{T}$ and $\mathbf{V}$ are the kinetic- and potential-energy operators, respectively. $i = \sqrt{-1}$, while $\hbar$ is Planck's constant divided by 2π. Plenty of numerical algorithms are available for the propagation of Eqn. 1. We chose Fleck *et al.* [19]'s split-operator Fourier method because its accuracy and efficiency have been thoroughly demonstrated over the past few decades, and also because it reinforces the mathematical structure of quantum mechanics and quantum chemistry [20–23]. Next we review their approach.

2.1 Wavefunction Propagation

Fleck *et al.* [19] began by formally integrating Eqn. 1 to get

$$\begin{aligned}\Psi(\mathbf{r},t+\Delta t) &= e^{-i\frac{\Delta t}{\hbar}\mathbf{H}}\Psi(\mathbf{r},t)\\ &= e^{-i\frac{\Delta t}{\hbar}(\mathbf{T}+\mathbf{V})}\Psi(\mathbf{r},t). \quad (2)\end{aligned}$$

Equation 2 is correct provided that $\mathbf{H}$ is time-independent, which is the case should the collision system be isolated from the outside world—and the case we'll treat here.[1] $\mathbf{T} = -\frac{\hbar^2}{2\mu}\nabla^2$ with $\nabla^2 \equiv \boldsymbol{\nabla}\cdot\boldsymbol{\nabla}$ being the divergence of the gradient, or Laplacian operator.[2] μ is the system's (often reduced) mass, and $\mathbf{V} = V(\mathbf{r})$ where $V(\mathbf{r})$ is the potential. These relations allow us to recast Eqn. 2 as

$$\begin{aligned}\Psi(\mathbf{r},t+\Delta t) &= e^{-i\frac{\Delta t}{\hbar}(\mathbf{T}+\mathbf{V})}\Psi(\mathbf{r},t)\\ &= e^{-i\frac{\Delta t}{\hbar}\left(-\frac{\hbar^2}{2\mu}\nabla^2+V(\mathbf{r})\right)}\Psi(\mathbf{r},t). \quad (3)\end{aligned}$$

Evaluation of Eqn. 3 is problematic, though, since it contains both differential and scalar parts mixed together in the same exponentiated operator. To fix this we might be tempted to isolate these parts from each other as

$$\begin{aligned}\Psi(\mathbf{r},t+\Delta t) &\approx e^{-i\frac{\Delta t}{\hbar}\mathbf{T}}e^{-i\frac{\Delta t}{\hbar}\mathbf{V}}\Psi(\mathbf{r},t)\\ &= e^{i\frac{\hbar\Delta t}{2\mu}\nabla^2}e^{-i\frac{\Delta t}{\hbar}V(\mathbf{r})}\Psi(\mathbf{r},t), \quad (4)\end{aligned}$$

and such an approach was employed by Hardin and Tappert several decades ago when they were handling nonlinear wave calculations [27].

But we must keep in mind that Eqn. 4 is just an approximation—not an equality. Exponentiated operators don't follow the familiar rule that $e^c = e^a e^b$ if $c = a + b$ when a, b, and c are functions. Instead the correct relationship is provided by the Baker-Campbell-Hausdorff (BCH) theorem, which says that when $\mathbf{A}$, $\mathbf{B}$, and $\mathbf{C}$ are operators $e^{\mathbf{C}} = e^{\mathbf{A}}e^{\mathbf{B}}$ if and only if

$$\begin{aligned}\mathbf{C} &= \mathbf{A}+\mathbf{B}\\ &+ \frac{1}{2}[\mathbf{A},\mathbf{B}]\\ &+ \frac{1}{12}([\mathbf{A},[\mathbf{A},\mathbf{B}]]+[[\mathbf{A},\mathbf{B}],\mathbf{B}])\\ &+ \frac{1}{48}([\mathbf{A},[[\mathbf{A},\mathbf{B}],\mathbf{B}]]+[[\mathbf{A},[\mathbf{A},\mathbf{B}]],\mathbf{B}])\\ &+ \frac{1}{120}([[\mathbf{A},[[\mathbf{A},\mathbf{B}],\mathbf{B}]],\mathbf{B}]+[\mathbf{A},[[\mathbf{A},[\mathbf{A},\mathbf{B}]],\mathbf{B}]])\\ &- \frac{1}{360}([\mathbf{A},[[[\mathbf{A},\mathbf{B}],\mathbf{B}],\mathbf{B}]]+[[\mathbf{A},[\mathbf{A},[\mathbf{A},\mathbf{B}]]],\mathbf{B}])\\ &- \frac{1}{720}([\mathbf{A},[\mathbf{A},[\mathbf{A},[\mathbf{A},\mathbf{B}]]]]+[[[[\mathbf{A},\mathbf{B}],\mathbf{B}],\mathbf{B}],\mathbf{B}])\\ &+ \cdots, \quad (5)\end{aligned}$$

where $[\mathbf{A},\mathbf{B}] \equiv \mathbf{AB}-\mathbf{BA}$ is the commutator of $\mathbf{A}$ and $\mathbf{B}$ [28–33].[3] We can see from the BCH theorem that Eqn. 4 has leading error $\mathcal{O}(\Delta t^2)$, where $\mathcal{O}$ means "on the order of."

Fleck *et al.* [19] made the important insight that we can easily do better than Eqn. 4 by splitting the exponentiated operator symmetrically as

$$\begin{aligned}e^{-i\frac{\Delta t}{\hbar}(\mathbf{T}+\mathbf{V})} &= e^{-i\frac{\Delta t}{\hbar}(\mathbf{V}+\mathbf{T})}\\ &\approx e^{-i\frac{\Delta t}{2\hbar}\mathbf{V}}e^{-i\frac{\Delta t}{\hbar}\mathbf{T}}e^{-i\frac{\Delta t}{2\hbar}\mathbf{V}}. \quad (6)\end{aligned}$$

This makes the first commutator in Eqn. 5 cancel, resulting in leading error $\mathcal{O}(\Delta t^3)$ [34]. The approximation of Eqn. 6 has the further advantage that it's unitary, and thus enhances numerical stability while enforcing norm conservation. Instead of Eqn. 4 we therefore get

$$\Psi(\mathbf{r},t+\Delta t) \approx e^{-i\frac{\Delta t}{2\hbar}V(\mathbf{r})}e^{i\frac{\hbar\Delta t}{2\mu}\nabla^2}e^{-i\frac{\Delta t}{2\hbar}V(\mathbf{r})}\Psi(\mathbf{r},t). \quad (7)$$

More elaborate splitting methods for the exponentiated operators can lead to cancellation of additional commutators in Eqn. 5, and thus even

[1] Equation 2 can be generalized to the case where the system is coupled to the outside world, making $\mathbf{H}$ time-dependent. $e^{-i(\Delta t/\hbar)\mathbf{H}}$ in Eqn. 2 would then be replaced by Dyson's expression $1+\sum_{j=1}^{\infty}(-i/\hbar)^j\int_0^t dt_1\int_0^{t_1}dt_2\cdots\int_0^{t_{j-1}}dt_j\mathbf{H}(t_1)\mathbf{H}(t_2)\cdots\mathbf{H}(t_j)$ which under the right circumstances reduces to $e^{-(i/\hbar)\int_0^t d\tau\,\mathbf{H}(\tau)}$ [24–26].

[2] An old-fashioned, but still occasionally used symbol for the Laplacian operator is $\triangle$.

[3] Mistakes can sometimes be found in published accounts of the BCH theorem—especially for the higher-order terms. To help clear them up Eqn. 5 contains far more terms than are customary, or really necessary here.

smaller leading error terms. But they often result in such large increases in computational time that they aren't of much practical benefit.[4] This is akin to what occurs with Runge-Kutta (RK) approximations for the solution of ordinary differential equations; there are possibilities for many different orders, but one order—for RK approximations the fourth—tends to be the most useful in practice [37].

To evaluate the exponentiated differential operator in Eqn. 7 Fleck *et al.* invoked the notion that differentiation in **r**-space is tantamount to multiplication in **k**-space, where $\mathbf{p} = \hbar\mathbf{k}$ is the system's linear momentum and **k** is its wavevector.[5] For the Fourier transform pair in n spatial dimensions

$$\Phi(\mathbf{k},t) \equiv \frac{1}{(2\pi)^{\frac{n}{2}}} \int_{\text{All Space}} d\mathbf{r}\, e^{-i\mathbf{k}\cdot\mathbf{r}} \Psi(\mathbf{r},t) \equiv \mathcal{F}^{-}(\Psi) \quad (8)$$

and

$$\Psi(\mathbf{r},t) \equiv \frac{1}{(2\pi)^{\frac{n}{2}}} \int_{\text{All Space}} d\mathbf{k}\, e^{i\mathbf{k}\cdot\mathbf{r}} \Phi(\mathbf{k},t) \equiv \mathcal{F}^{+}(\Phi) \quad (9)$$

we have

$$\mathcal{F}^{\pm}\left(\boldsymbol{\nabla}\Psi\right) = (\mp i\mathbf{k})\mathcal{F}^{\pm}(\Psi), \quad (10)$$

which can be shown by partial integration [40].[6] Here $\Phi(\mathbf{k},t)$ is the wavefunction in **k**-space. Appealing to the series expansion defining an exponentiated operator we get

$$\begin{aligned} \mathcal{F}^{\pm}(e^{\nabla^2}\Psi) &= \mathcal{F}^{\pm}(e^{\boldsymbol{\nabla}\cdot\boldsymbol{\nabla}}\Psi) \\ &= e^{(\mp i\mathbf{k})\cdot(\mp i\mathbf{k})}\mathcal{F}^{\pm}(\Psi) \\ &= e^{-k^2}\mathcal{F}^{\pm}(\Psi), \end{aligned} \quad (11)$$

where $k^2 \equiv \mathbf{k}\cdot\mathbf{k}$.[7]

All this allows Eqn. 7 to be recast as

$$\begin{aligned} \Psi(\mathbf{r},t+\Delta t) \approx\ & e^{-i\frac{\Delta t}{2\hbar}V(\mathbf{r})}\mathcal{F}^{+}\left(e^{-i\frac{\hbar\Delta t}{2\mu}k^2}\right. \\ \cdot\ & \left.\mathcal{F}^{-}\left(e^{-i\frac{\Delta t}{2\hbar}V(\mathbf{r})}\Psi(\mathbf{r},t)\right)\right). \end{aligned} \quad (12)$$

Chaining M successive iterations of Eqn. 12 together and removing unnecessary parentheses as

$$\begin{aligned} \Psi(\mathbf{r},t+M\Delta t) \approx\ & e^{-i\frac{\Delta t}{2\hbar}V(\mathbf{r})} \\ \cdot\ & \left(\prod_{j=1}^{M-1}\mathcal{F}^{+}e^{-i\frac{\hbar\Delta t}{2\mu}k^2}\mathcal{F}^{-}e^{-i\frac{\Delta t}{\hbar}V(\mathbf{r})}\right) \\ \cdot\ & \mathcal{F}^{+}e^{-i\frac{\hbar\Delta t}{2\mu}k^2}\mathcal{F}^{-}e^{-i\frac{\Delta t}{2\hbar}V(\mathbf{r})}\Psi(\mathbf{r},t) \end{aligned} \quad (13)$$

eliminates computational redundancy, which can result in time savings and reduce roundoff error during calculations. Equations 12 and 13 are what our software evaluates to propagate wavefunctions.

2.2 Determination of Bound-State Energy Eigenvalues

Bound-state energy eigenvalues and the corresponding position-space eigenfunctions of the Hamiltonian operator can be recovered from the propagated wavefunction, should there be any. Most of the time there are for a potential with at least one local minimum, but not always [42]. To get them we use the temporal autocorrelation function

$$\mathcal{T}(t) \equiv \int_{\text{All Space}} d\mathbf{r}\, \Psi^{*}(\mathbf{r},0)\Psi(\mathbf{r},t), \quad (14)$$

which we form from wavefunctions saved during our propagation.

Remember that any wavefunction $\Psi(\mathbf{r},t)$ can be expanded in the complete set of orthonormal functions $\psi_n^m(\mathbf{r})$ of **H**;[8]

$$\Psi(\mathbf{r},t) = \sum_{m,n} A_n^m \psi_n^m(\mathbf{r}) e^{-i\frac{E_n}{\hbar}t}. \quad (15)$$

Here the index m covers any degeneracy present. This

[4] *E.g.*, Ruth showed that with leading error term $\mathcal{O}(\Delta t^4)$, $e^{\mathbf{A}+\mathbf{B}} \approx e^{\frac{7}{24}\mathbf{A}}e^{\frac{2}{3}\mathbf{B}}e^{\frac{3}{4}\mathbf{A}}e^{-\frac{2}{3}\mathbf{B}}e^{-\frac{1}{24}\mathbf{A}}e^{\mathbf{B}}$ [35, 36].

[5] **k**-space is often called "reciprocal space," especially in condensed-matter physics [38, 39].

[6] Use of "plus" and "minus" signs and of the often fractional power of "2π" for normalization in Eqns. 8 and 9 varies among mathematics and the different branches of science and engineering. Our symmetric normalization and use of the symbols "$\mathcal{F}^{+}$" and "$\mathcal{F}^{-}$" will hopefully help clear up any resulting ambiguities.

[7] An especially transparent derivation of this was provided by DeVries and Hasbun [41].

[8] In quantum chemistry and quantum mechanics it's commonplace to just presume that the $\psi_n^m(\mathbf{r})$ form a complete set, and leave the often arduous proof of completeness to mathematicians. Incomplete and overcomplete sets are also possibilities, along with contributions to our expansion from eigenfunctions with continuous eigenvalues. But handling them is beyond the scope of what we're doing here [43–47].

leads to

$$\begin{aligned}
\mathcal{T}(t) &\equiv \int_{\text{All Space}} d\mathbf{r}\, \Psi^*(\mathbf{r},0)\Psi(\mathbf{r},t) \\
&= \int_{\text{All Space}} d\mathbf{r} \sum_{m,n} A^{*m}_{\ n} \psi^{*m}_{\ n}(\mathbf{r}) e^{i\frac{E_n}{\hbar}(0)} \\
&\cdot \sum_{m',n'} A^{m'}_{n'} \psi^{m'}_{n'}(\mathbf{r}) e^{-i\frac{E_{n'}}{\hbar}t} \\
&= \sum_{m,n,m',n'} A^{*m}_{\ n} A^{m'}_{n'} e^{-i\frac{E_{n'}}{\hbar}t} \\
&\cdot \int_{\text{All Space}} d\mathbf{r}\, \psi^{*m}_{\ n}(\mathbf{r}) \psi^{m'}_{n'}(\mathbf{r}) \\
&= \sum_{m,n,m',n'} A^{*m}_{\ n} A^{m'}_{n'} e^{-i\frac{E_{n'}}{\hbar}t} \delta_{m,m'}\delta_{n,n'} \\
&= \sum_{m,n} |A^m_n|^2 e^{-i\frac{E_n}{\hbar}t} \\
&= \sum_n B_n e^{-i\frac{E_n}{\hbar}t}, \qquad (16)
\end{aligned}$$

where $\delta_{j,j'}$ is Kronecker's delta, and $B_n \equiv \sum_m |A^m_n|^2$ quantifies the admixture of degenerate states in the n^{th} energy eigenfunction.[9] Equation 16's one-dimensional Fourier transform is the energy spectrum

$$\begin{aligned}
\mathcal{E}(E) &\equiv \mathcal{F}^+\mathcal{T} \\
&= \frac{1}{\sqrt{2\pi}} \int_{-\infty}^{\infty} dt\, e^{i\frac{E}{\hbar}t} \sum_n B_n e^{-i\frac{E_n}{\hbar}t} \\
&= \sum_n B_n \frac{1}{\sqrt{2\pi}} \int_{-\infty}^{\infty} dt\, e^{i\frac{E-E_n}{\hbar}t} \\
&= \sqrt{2\pi} \sum_n B_n \delta\left(\frac{E-E_n}{\hbar}\right), \qquad (17)
\end{aligned}$$

where we've used

$$\delta\left(\frac{E-E_n}{\hbar}\right) = \frac{1}{2\pi}\int_{-\infty}^{\infty} dt\, e^{i\frac{E-E_n}{\hbar}t} \qquad (18)$$

as a representation of the Dirac-delta function [50–54].

The Dirac-delta functions in Eqn. 17 will invariably be broadened, as in our situation $\mathcal{T}(t)$ isn't defined over an infinite interval. Rather it's defined only over the period from 0 to T, where T is the maximum time that $\Psi(\mathbf{r},t)$ is calculated at. Rather than increase T to minimize the broadening so that the values for the set of E_n can be determined, it's more efficient to multiply $\mathcal{T}(t)$ before Fourier transforming by the Hanning (more properly called the Hann, and often confused with the Hamming) window function[10]

$$w(t) = \frac{1}{T}\left(1 - \cos\left(\frac{2\pi t}{T}\right)\right). \qquad (19)$$

Each Dirac-delta function in the energy spectrum then becomes

$$\begin{aligned}
\mathcal{L}\left(\frac{E-E_n}{\hbar}\right) &= \int_0^T dt\, w(t) e^{i\frac{E-E_n}{\hbar}t} \\
&= \int_0^T dt\, \frac{1}{T}\left(1 - \cos\left(\frac{2\pi t}{T}\right)\right) \\
&\cdot\ e^{i\frac{E-E_n}{\hbar}t} \\
&= \int_0^T dt\, \frac{1}{T}\left(1 - \frac{e^{i\frac{2\pi t}{T}} + e^{-i\frac{2\pi t}{T}}}{2}\right) \\
&\cdot\ e^{i\frac{E-E_n}{\hbar}t} \\
&= \frac{1 - e^{i\frac{E-E_n}{\hbar}T}}{\frac{E-E_n}{\hbar}T} i \\
&- \frac{1}{2}\left(\frac{1 - e^{i\frac{E-E_n}{\hbar}T + 2\pi}}{\frac{E-E_n}{\hbar}T + 2\pi}\right. \\
&+ \left.\frac{1 - e^{i\frac{E-E_n}{\hbar}T - 2\pi}}{\frac{E-E_n}{\hbar}T - 2\pi}\right) i. \qquad (20)
\end{aligned}$$

This changes the spectrum into

$$\mathcal{E}(E) = \sqrt{2\pi}\sum_n B_n \mathcal{L}\left(\frac{E-E_n}{\hbar}\right). \qquad (21)$$

To determine the maxima in Eqn. 21—the energy eigenvalues we want—we could use standard least-squares lineshape fitting techniques [56, 57]. But such sophistication usually isn't warranted when the eigenvalues are well separated. In these cases an analytic three-point fit to each maximum will normally suffice. Equation 21 is represented in our software by an array of values at intervals separated by energy increment ΔE. A true local maximum of the spectrum will almost never be located exactly at one of these array points, but rather between two successive points. Feit and Fleck showed that if we determine a peak of a spectrum represented in an array, then we can determine δ_{offset}—the separation a real peak lies from it—by a simple procedure stemming from some algebra applied to the analytic form of the lineshape function:

[9] Here and in what follows we must be careful about the legitimacy of interchanging the order of integration and summation [48, 49].

[10] Harris has thoroughly discussed the advantages and disadvantages of various window functions for use in discrete Fourier analysis [55].

- form the ratio $R \equiv \mathcal{E}(E_{j+1})/\mathcal{E}(E_{j-1})$ where j is the array element containing the local maximum,
- compute $r \equiv (1+R)/(1-R)$, and
- determine the offset as

$$\delta_{\text{offset}} = \begin{cases} \pi\left(-3r + \sqrt{9r^2-8}\right)/T & \text{if } R < 1, \text{ or} \\ \pi\left(-3r - \sqrt{9r^2-8}\right)/T & \text{if } R > 1. \end{cases} \tag{22}$$

The energy eigenvalue E_n we're after then becomes $E_n = \mathcal{E}(E_j) - \delta_{\text{offset}}$ [58].

2.3 Determination of Bound-State Position-Space Energy Eigenfunctions

With the set of bound-state energy eigenvalues in hand we can go on to figure out the corresponding bound-state energy eigenfunctions in position space. For this we again recall that the position-space wavefunction at any time can be expanded in terms of them; $\Psi(\mathbf{r},t) = \sum_{m,n} A_n^m \psi_n^m(\mathbf{r}) e^{-i\frac{E_n}{\hbar}t}$. Temporal integration over both sides of this with $e^{i\frac{E}{\hbar}t}w(t)$ gives

$$\begin{aligned} \Upsilon(\mathbf{r},E) &\equiv \int_0^T dt\, e^{i\frac{E}{\hbar}t} w(t) \Psi(\mathbf{r},t) \\ &= \int_0^T dt\, e^{i\frac{E}{\hbar}t} w(t) \\ &\quad \cdot \sum_{m,n} A_n^m \psi_n^m(\mathbf{r}) e^{-i\frac{E_n}{\hbar}t}. \end{aligned} \tag{23}$$

By integrating over time we've converted our time-dependent wavefunction $\Psi(\mathbf{r},t)$ into an energy-dependent wavefunction $\Upsilon(\mathbf{r},E)$. Equation 23 reduces to

$$\begin{aligned} \Upsilon(\mathbf{r},E) &= \sum_{m,n} A_n^m \psi_n^m(\mathbf{r}) \int_0^T dt\, e^{i\frac{E-E_n}{\hbar}t} w(t) \\ &= \sum_{m,n} A_n^m \psi_n^m(\mathbf{r}) \mathcal{L}\left(\frac{E-E_n}{\hbar}\right). \end{aligned} \tag{24}$$

Noting that $\lim_{E\to 0} \mathcal{L}(E/\hbar) = 1$ and assuming the bound-state eigenenergies are well-separated, we get to good approximation for the choice $E = E_n$ that Eqn. 24 collapses into

$$\Upsilon(\mathbf{r},E_n) \approx \sum_m A_n^m \psi_n^m(\mathbf{r}). \tag{25}$$

But by Eqn. 23 this becomes

$$\sum_m A_n^m \psi_n^m(\mathbf{r}) \approx \int_0^T dt\, e^{i\frac{E_n}{\hbar}t} w(t) \Psi(\mathbf{r},t). \tag{26}$$

Equation 26 is therefore our prescription for getting the superposition over all the degenerate wavefunctions present for the n^{th} energy level. It *looks* like another Fourier transform, but since E_n is a constant—not a variable—it really isn't. In practice we calculate Eqn. 26 using the trapezoid rule [59, 60].

For one spatial dimension, the issue of degeneracy is irrelevant. The bound states of such systems are always non-degenerate [61]. Equation 26 thus gives the single eigenfunction we want, to within a normalization factor that can be easily determined numerically at our convenience. But for multiple spatial dimensions degenerate levels become a problem; how do we separate their eigenfunctions from each other? The solution to this problem turns out to be simple. Remember that degeneracy usually arises from symmetry present in **H**, and that symmetry is conserved when a wavefunction is propagated over time [62–64]. So we identify the relevant symmetries, and do multiple propagations starting with wavefunctions of the right symmetry for each case to ensure that only eigenfunctions of the correct symmetry are present when evaluating Eqn. 26.[11]

2.4 Computational Implementation

The software we developed to implement the theoretical approach just described relies heavily on evaluating Fourier integrals like those in Eqns. 8 and 9. We therefore need a method to compute such integrals quickly and accurately. Of course this method is the Fast Fourier Transform (FFT) algorithm. It's one of the most significant advances in numerical analysis made during the twentieth century, although at least parts of it were discovered independently by several people starting just after the beginning of the nineteenth century [67, 68]. It came into widespread use after the middle nineteen-sixties, when Cooley and Tukey published a research article highlighting its efficiency and precision and also showing in an organized way how the various techniques needed for its implementation fit together [69]. The FFT can be performed in as many dimensions as we want—as long as we stick with Cartesian (or "rectangular") coördinates.[12] But it's easiest to understand by thinking in just one spatial dimension—so our treatment of it will be one-dimensional. Following

[11] Unfortunately, symmetries aren't always completely obvious, like the Laplace-Runge-Lenz symmetry of the hydrogen atom [65, 66].

[12] How to handle the FFT in non-Cartesian coördinate systems is a whole another story, and one we won't get into here.

common usage we therefore relabel $\mathbf{r}$ as x, and $\mathbf{k}$ as k.

The FFT doesn't actually calculate Fourier integrals, but quantities very much *like* them—sets of numbers which scale as Fourier series expansion coefficients [70, 71]. When provided with a function $\Psi(x,t)$ sampled at N points stored in an array, the FFT returns the same array filled with the N scaled expansion coefficients which comprise the approximation for $\Phi(k,t)$. By conventional methods it would take $\mathcal{O}(N^2)$ operations to perform such calculations. But the FFT exploits the periodicity of complex exponential functions—or equivalently, the sines and cosines which make them up—to reduce the number of operations to $\mathcal{O}(N \log_2 N)$. When N becomes large this reduction in computational time becomes tremendous. For example, when $N = 2^9 = 512$ the FFT gives a computational time reduction of about 99% compared to conventional means. When $N = 2^{16} = 65536$ this reduction increases to around 99.99%, and it only gets better as N goes up! The reduction in the number of operations required by the FFT has another advantage—minimization in the build up of numerical roundoff error.

But the speed and accuracy afforded by the FFT come with a cost that's a result of the periodicity of complex exponential functions—and we have no choice about it.[13] This periodicity makes the FFT presume the functions it approximates to also be periodic—even when they're not—which leads to important consequences.

In x-space the periodicity means that the bounds of Eqn. 8 aren't really from $-\infty$ to ∞, but rather from some $x_{\min.}$ to some other $x_{\max.}$, both of our choosing. The first element of the array containing the function to be transformed therefore stores the value $\Psi(x_{\min.},t)$. Subsequent array elements hold $\Psi(x,t)$ evaluated at values of x which are incremented by Δx, where

$$\Delta x = \frac{x_{\max.} - x_{\min.}}{N}. \tag{27}$$

The last array element contains $\Psi(x_{\min.} + (N-1)\Delta x, t)$, not $\Psi(x_{\max.},t)$. The presumed periodicity means that $\Psi(x_{\max.}) = \Psi(x_{\min.})$—the value stored in the first array element. Such a scheme is spelled out in Table 1. When a wavefunction moves off one end of the array it therefore "wraps around" to the other end. This can lead to one end of the wavefunction artificially interfering with the other end, and is usually easy to recognize just by watching the wavefunction evolve in position space. A cure to it is also easy to implement—simply choose the region of position space to be large enough that the wavefunction doesn't wrap around during the computation!

The assumed periodicity also applies to k-space. But here it's more subtle, and easier to miss. Just as the FFT doesn't cover $-\infty$ to ∞ in x-space, it only covers a finite range of k-space—the one from $-k_{\text{Nyqt.}}$ to $k_{\text{Nyqt.}}$ in increments of

$$\begin{aligned} \Delta k &= \frac{2\pi}{N\Delta x} \\ &= \frac{2\pi}{x_{\max.} - x_{\min.}}. \end{aligned} \tag{28}$$

Here $k_{\text{Nyqt.}} = \pi/\Delta x$ is called the *Nyquist* wavenumber [74, 75].

What complicates the FFT's usage even more is that it stores its k-space representation of the function in a rather non-intuitive fashion with the negative wavenumbers placed *after* the positive ones. This is also shown in Table 1.[14] If the expansion coefficients for $|k| > k_{\text{Nyqt.}}$ are zero, then the function is called *band-limited* and the FFT's representation of it is exact to within roundoff error. But if not then we run into a problem—we get wrap-around again. This time the FFT erroneously maps the nonzero $|k| > k_{\text{Nyqt.}}$ expansion coefficients back into the range $-k_{\text{Nyqt.}} < k \leq k_{\text{Nyqt.}}$, corrupting the function's representation. Such errors are called *aliasing*, and are probably the most common mistakes made when using the FFT. Again the remedy is to choose a region of k-space large enough to accommodate all nonzero expansion coefficients.[15] But sometimes implementing this remedy can be tricky, since the regions of x- and k-space used are intertwined through Eqns. 27 and 28.

Another common mistake made when using the

[13] *Cf.*, the *principal value* of a complex number, how it's related to the point it represents in the complex plane, and the infinite number of other values that could be used to represent the same point in the complex plane [72, 73].

[14] If such the storage arrangement in k-space is simply too confusing, then the FFT's output can be reordered, worked on as needed, and then put back in order before sending it back to the FFT. But we chose not to do so here because it leads to extra computer operations.

[15] If $\Phi(k,t)$ is localized near k_0 where k_0 is outside the region of reciprocal space covered by the FFT, then we can multiply by e^{-ik_0x} before transforming to k-space to move the function into the proper range, do the required operations on it, transform back to x-space and then multiply the result by e^{ik_0x}. This comes from the Fourier transform shifting theorem, which says that if $\Phi(k,t) = \mathcal{F}^-(\Psi(x,t))$ and $\Psi(x,t) = \mathcal{F}^+(\Phi(k,t))$, then $\Phi(k+k_0,t) = \mathcal{F}^-\left(e^{-ik_0x}\Psi(x,t)\right)$ and $\Psi(x+x_0,t) = \mathcal{F}^+\left(e^{ikx_0}\Phi(k,t)\right)$ [76]. Physically this amounts to making Galilean transformations [77].

Table 1. Details of how the FFT stores data in an array of N elements. The top row provides the index numbers for the elements in Fortran; in computer languages like C the numbering would start with zero. The "$\pm$" for the k-value of element $N/2+1$ comes from the periodicity built into the FFT; $\pm\,(N/2)\,\Delta k$ are effectively the same number from its viewpoint, just like $x_{\max.}$ and $x_{\min.}$. Note that once determined, values like $x_{\max.}$, $x_{\min.}$, Δx and Δk are never actually presented to the FFT, but N is.

Array Element	1	2	...	$\frac{N}{2}$	$\frac{N}{2}+1$	...	$N-1$	N
x-value	$x_{\min.}$	$x_{\min.}+\Delta x$	...	$x_{\min.}+\left(\frac{N}{2}-1\right)\Delta x$	$x_{\min.}+\left(\frac{N}{2}\right)\Delta x$	...	$x_{\min.}+(N-2)\Delta x$	$x_{\min.}+(N-1)\Delta x$
k-value	0	Δk	...	$\left(\frac{N}{2}-1\right)\Delta k$	$\pm\left(\frac{N}{2}\right)\Delta k$	...	$-2\Delta k$	$-\Delta k$

FFT is called *leakage*. When periodic functions are given to the FFT for only a partial period of them an "artificial" discontinuity is created where the function wraps around. To try to represent this artificial discontinuity the FFT erroneously "leaks" values into Fourier expansion components near where they should have been. One way to minimize the resulting problems is to somehow get rid of the artificial discontinuity. This is effectively what we did previously when we multiplied by the Hann window function before Fourier transforming to calculate eigenvalues and eigenfunctions [78].

Without reasonably chosen parameters, no numerical method will produce reasonable results. For us this clearly includes choosing the range in position space so that wrap around is negligible, while ensuring that the wavefunction is adequately sampled and doesn't get aliased in k-space. But there's more to it than just that. Time and energy are conjugate variables and are also often involved in the FFT calculations we need to do. Of course we also need to choose them so that aliasing doesn't occur. The potential is critical here. Let's imagine that for the domain in position space we choose its values span the range $\Delta V = V_{\max.} - V_{\min.}$, where $V_{\max.}$ and $V_{\min.}$ are its maximum and minimum values, respectively. Then at the very least we must choose $\Delta t < \pi/\Delta V$, or aliasing will occur. Good results will almost certainly be produced when Δt is less than $1/4$ this value. The resolution we can determine energy eigenvalues with is also affected; with ΔE this resolution, we have $\Delta E = \pi/T$ where $T = J\Delta t$ is the time interval encompassing the propagation and J is the number of temporal steps in the propagation. Use of the analytic lineshape fitting we described before can improve this resolution substantially. The accuracy of our results is also related to the continuity of the various functions being numerically described, and will be addressed shortly.

The FFT we employed here requires the number of array elements for wavefunction representation to be an integral power of two and is thus known as a *radix-two* FFT. We chose this type of FFT because it's the simplest and commonest of them. Other possibilities are available, and occasionally the small gains in efficiency they provide justify their use, but we won't get into the added complications that come with them here [79].

Our source code was written in Fortran. Both venerable and obsolete, Fortran has the advantages of having very natural syntax for representing equations, has complex number data types built in, and runs quite fast [80]. Fortran has experienced a resurgence of popularity in recent years, partly due to the practical necessity of having a high-performance "number crunching" computer language like it to support artificial intelligence [81]. Translation of our Fortran source code to other languages like C, C++, or Python is straightforward—and makes an excellent programming exercise to enhance the understanding of the detailed workings of our source code!

All source code for computations—including for the FFT—can be downloaded as noted in the Introduction of this article. Graphics were produced by calls to PlPlot subroutines, and the PlPlot freeware package is widely available for download. We used the GNU Fortran compiler, which can also be easily downloaded. With the computers characterized in Table 2 the program typically runs in seconds to minutes—even on the more modest of the two of them.[16] Double-precision arithmetic was employed, though the source code can be easily modified to support arbitrary levels of precision. Our

[16]Sometimes the software runs so fast that the graphics develop too rapidly to easily follow. The easiest way to fix this is to increase the number of elements in the array containing the wavefunction and to put in more hidden propagations using Eqn. 13, keeping the computer busier in between displaying frames.

Table 2. Important characteristics of the computers used for calculations. Here the abbreviations "Mfgr" mean commercial producer, "CPU" central processing unit,"RAM" random access memory, and "HD" hard drive. "GHz" means gigahertz, while "GB" stands for gigabytes, and "TB" denotes terabytes.

Mfgr	Model	CPU	Clock Speed	RAM	HD Type and Capacity	Operating System
Dell	Inspiron 17 3793	Intel Core i3 1005G1, 2 Cores	1.20 GHz	8 GB	Rotary-Magnetic, 1 TB	Microsoft Windows 10, Version 2009, 64-bit
Dell	Inspiron 15 5155	AMD Ryzen 7 5700U, 8 Cores	1.80 GHz	16 GB	Solid-State, 1 TB	Microsoft Windows 11, Version 22H2, 64-bit

programming was done using "natural" units where $\hbar = c = e = 1$. Here c is the speed of light and $-e$ is the electron's charge [82, 83].

Though our software is made to show wavefunctions visually, a graphical-user interface (GUI) was deliberately left out, requiring the user to make changes at the source-code level and recompile after each modification. Such an approach motivates the user to understand how the source code works; inclusion of a GUI would make it easy to ignore the "nuts and bolts" underlying our software.

3 Discussion of Results

Now that we've covered the theoretical underpinnings and computational implementation of our source code, we go on to treat its use for describing various physical systems. We start with a simple system, and then move on to a more complicated one.

Since we intuitively conceive of collisions in terms of what's happening before, during, and after the involved particles hit each other, we need a wavefunction that represents a particle localized about a point in position space prior to the collision. Of the many possibilities available we chose the normalized Gaussian wavefunction

$$\Psi(\mathbf{r},0) = \frac{1}{\left(\sigma\sqrt{2\pi}\right)^{\frac{n}{2}}} e^{-\frac{(\mathbf{r}-\mathbf{r}_0)^2}{4\sigma^2}+i\mathbf{k}_0\cdot\mathbf{r}}. \qquad (29)$$

Here $\mathbf{r}_0$ is the wavefunction's center, σ characterizes its width in position space, and $\mathbf{k}_0$ is the mean wavevector for the particle it describes.[17]

[17]Gaussian wavefunctions aren't band-limited, so they do lead to aliasing and potentially leakage. But if parameters are chosen properly the resulting perspective produced are negligible.

We chose a Gaussian wavefunction instead of others available because Gaussian wavefunctions correspond to the minimum uncertainty possible according to Heisenberg's uncertainty principle [84]. For our case of $n = 1$ spatial dimension, Eqn. 29 becomes

$$\Psi(x,0) = \frac{1}{\sqrt{\sigma\sqrt{2\pi}}} e^{-\frac{(x-x_0)^2}{4\sigma^2}+ik_0x}, \qquad (30)$$

where x replaces $\mathbf{r}$, x_0 replaces $\mathbf{r}_0$ and k_0 replaces $\mathbf{k}_0$.

3.1 Simple Scattering from a Rectangular Barrier

The first results we present are for scattering from a rectangular barrier—which amounts to just about the simplest one-dimensional collision system there is. We start with it not due just to its simplicity, but also because it allows direct comparison with the results of Goldberg, Schey, and Schwartz (GSS) [85]. Theirs are possibly the first widely known calculations of wavefunctions for collisions whose results were provided as motion pictures ("movies"). Because of format constraints they were able only to display "frames" of these movies in their journal publication. To get the actual movies GSS or their representatives would need to be contacted. We face similar constraints here, and thus show only corresponding frames from our movies. But the miniaturization, increases in capability, and decreases in cost of computers over the decades makes the process of getting the movies much easier. Our software can be downloaded and compiled rapidly, and—like we said—calculate wavefunctions and display their evolution as movies in a matter

of seconds to minutes even on computers which are modest by current standards.

The parameters we chose mostly mimic GSS's deliberately. Our range for representing the wavefunction in position space was 1, and the absolute value of our potential's maximum was $V_0 = 2(50\pi)^2$. Our potential was centrally placed, and had a half-width of 0.032. The initial Gaussian wavefunction we used had a characteristic width 5% the range of position space, and was started $1/4$ the way along this range with $k_0 = 100\pi$.[18] The particle our wavefunction described had mass $1/2$, and the time step for propagation we employed was $5 \cdot 10^{-7}$. The only difference between our parameters and theirs was the size of the array used to represent the wavefunction. Theirs had 2000 elements; we had to choose the closest integral power of 2 to this, which was $2^{11} = 2048$.

Figure 1 shows our results, and corresponds to GSS's Figure 6. Both are read by going from left-to-right and then back to the beginning of the next row like a page in English is read. Like them, we display not the position-space wavefunction itself but rather the probability density corresponding to it. Also like them we superimposed the potential on top of the probability density. For easy comparison of our and their results we clipped out the first and last eighth of position space. Their and our results agree quite well frame-by-frame. As the probability density approaches the barrier, it broadens like the uncertainty principle demands. Once it impinges on the barrier reflections occur. These reflections make the wavefunction interfere with itself and are what cause the peaks and valleys in the probability density as it passes through the potential.

Once no longer in the barrier, the probability density regains its original shape along with broadening some more, reforming in two separate places. One of them is to the right of the barrier, where we expect—as the kinetic energy of the incoming particle is twice the maximum potential energy of the barrier. The other is to barrier's left, and is due to partial reflection. Such quantum-mechanical results of course go against what classical mechanics predicts. The latter says the particle either goes through the barrier or doesn't, depending on its energy. The interference we see in Figure 1 is akin to what happens in the diffraction of

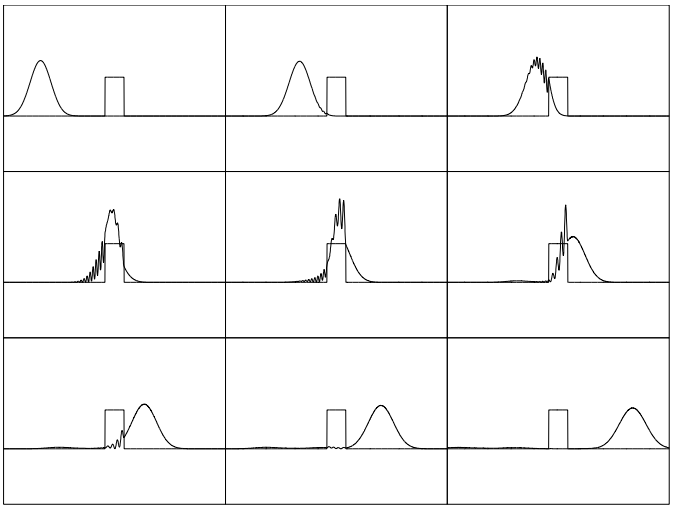

Figure 1. Scattering of a particle from a rectangular barrier for the parameters used by GSS in Figure 6 of their article. The times for the snapshots shown here match theirs: 0, 400, 560, 800, 900, 1040, 1200, 1360 and 1680. Here and in the next few figures horizontal axes represent position x while vertical axes indicate probability density $\Psi^*(x,t)\Psi(x,t)$. Note how diminished the reflected portion of the wavefunction is compared to the transmitted portion.

light in the double-slit experiment or the diffraction of X-rays by crystals often treated in elementary chemistry and physics courses [86, 87]. In those cases the diffraction pattern persists, but for our situation the diffraction pattern resolves itself quickly after forming.

3.2 Resonant Scattering from a Rectangular Barrier

We compare our results to GSS's again in Figure 2, which corresponds to their Figure 5(a, b). All the parameters used matched theirs when possible, which amounted to changing the range for representing the wavefunction in position space to $5/\sqrt{2} \approx 3.5$ and k_0 to $50\sqrt{2}\pi \approx 70.7\pi$. This time they used a 5000 element array to express the wavefunction; ours was the closest integral power of 2 to this, which was $2^{12} = 4096$. Our time step matched theirs at $2 \cdot 10^{-6}$. Figure 2 tracks frame-by-frame quite well with their results and has some of the same features that our Figure 1 does: transmission and reflection, and interference in the vicinity of the barrier.

But this time there's something additional going on. Part of the probability density temporarily gets "stuck" inside the barrier, seemingly sloshing back and forth while it slowly leaks out. This is called a *resonance*. Resonances only happen when the energy of the incoming wavefunction is just right, and they can change the outcomes of collisions tremendously—enhancing the possibility of atoms, molecules, and nuclei being excited from their ground

[18] GSS used a "2" in the exponential part of their formula for a Gaussian wavefunction in place of our corresponding "4" in Eqns. 29 and 30. Their σ_0 thus differs from our σ by a factor of $\sqrt{2}$.

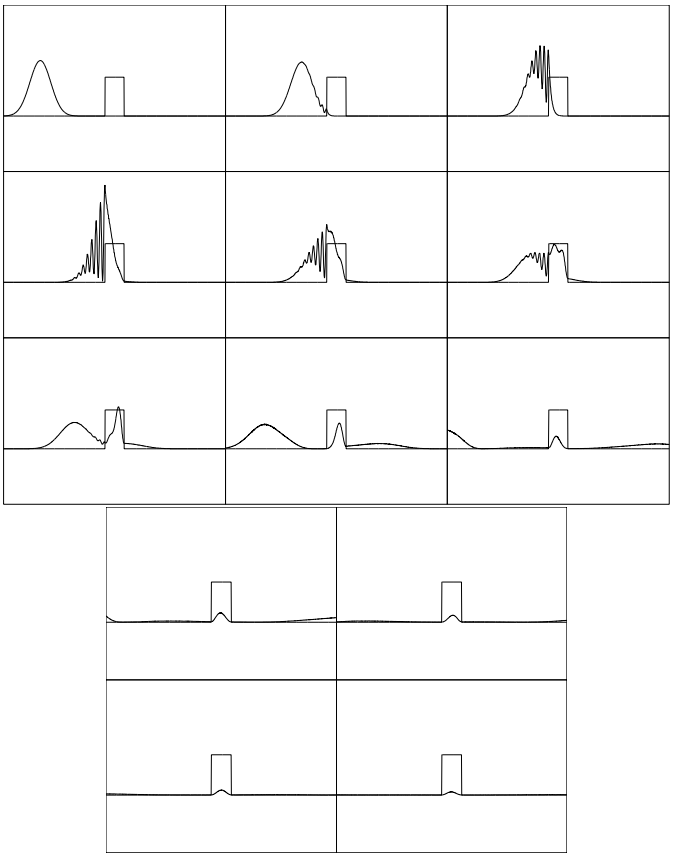

Figure 2. Scattering of a particle from a rectangular barrier for the parameters used by GSS in Figures 5(a, b) of their article. The time values for the frames are the same as GSS's: 0, 300, 400, 600, 650, 700, 800, 1050, 1450, 1600, 1850, 2100 and 2450.

to higher states during collisions. Resonances can be classified into different types [88–91]. The one we see here is called a *shape* resonance, as the shape of the potential is what leads to the temporary trapping of the particle.

3.3 Scattering from a Rectangular Well

Figure 3 provides our next comparison to GSS's results. It treats scattering from a rectangular well—Figure 1 in their article. Again we went with parameters that mimic theirs so that the comparison would be meaningful. They chose an array of 1000 elements for the wavefunction; we had to settle with $2^{10} = 1024$. Like them we also set the range this array covered in position space back to 1, made the potential negative to create a well rather than a barrier, put the incoming wavenumber of the particle the wavefunction described to 50π, and set the time increment to $2 \cdot 10^{-6}$.

When looked at coarsely, our results match up well with theirs. But a closer look reveals a crucial difference. In the later stages of the collision both the

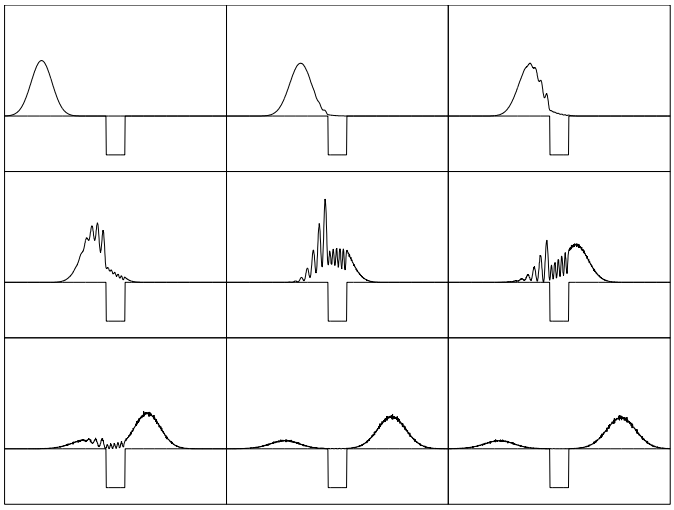

Figure 3. Scattering from a rectangular well. The time values were 0, 200, 240, 280, 360, 440, 520, 640 and 680.

transmitted and reflected portions of our probability density look like two hills covered with uncut grass! This is a deficiency in our calculation, not theirs.

What's the problem here? Recall that our approach hinges on Fourier expansions. When used to represent a discontinuity such expansions converge in the mean but tend to overshoot or undershoot correct values depending on which side the discontinuity is approached from.[19] While the wavefunction we're working with is continuous, the potential we're coupling it to throughout our calculations isn't. On top of this, the discrete representation of mathematical functions in arrays mandated by computer languages like Fortran makes it ambiguous where a discontinuity is. It's between the array element lower than the discontinuity and the array element higher, but exactly where in between?

There are several natural remedies to our problem: we could choose larger array sizes to force better localization of discontinuities, or choose smaller time steps to minimize the error present in Eqns. 12 and 13. We could also modify the discontinuity by representing it by the average of the two different values bracketing the discontinuity at an array element between the ones where the discontinuity occurs—effectively forcing continuity by modifying the function being represented. Our software allows for all three approaches in combination if needed. Here, it was sufficient to reduce the time step by an order of magnitude to $2 \cdot 10^{-7}$. The resulting solution, shown in Figure 4, is essentially free of noticeable "grass."

[19] *I.e.*, Gibbs's phenomenon [92, 93].

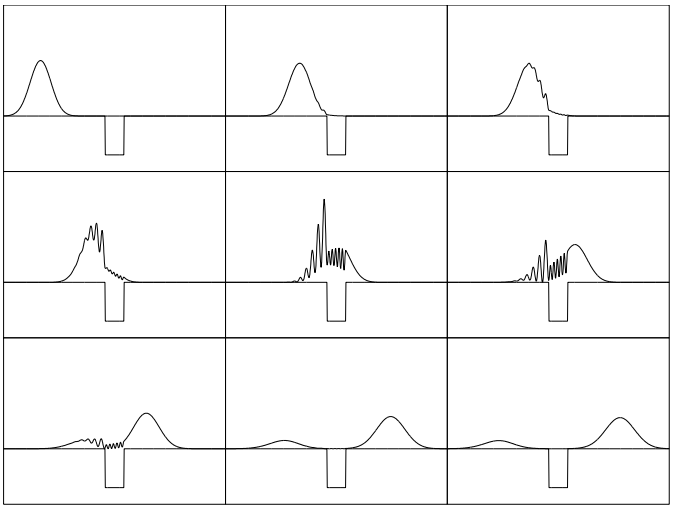

Figure 4. Scattering from a rectangular well again. The time values were 0, 200, 240, 280, 360, 440, 520, 640 and 680.

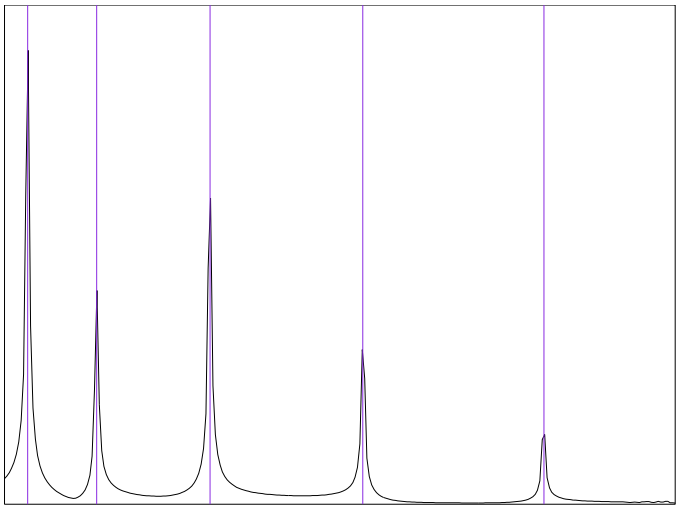

Figure 5. The bound-state energy eigenvalue spectrum for our rectangular well. Along the vertical axis is $\mathcal{E}$ as defined in Eqn. 21. On the horizontal axis is energy—our software automatically scales this axis to cover only the bound-state energy range. The height of each peak is proportional to the fraction of the corresponding eigenfunction in the propagating wavefunction. Often the vertical axis for spectra is logarithmic to allow spectral peaks of a variety of heights to be easily viewed simultaneously. Here the range of peak heights was small enough to make this unnecessary; the vertical scale is linear.

3.4 Determination of Bound-State Energy Eigenvalues and Position-Space Energy Eigenfunctions for a Rectangular Well

Like we detailed previously, our source code allows us to go beyond what GSS accomplished and to determine any bound-state energy eigenvalues that might exist along with their corresponding position-space energy eigenfunctions. Figure 5 shows the former calculated by our computer program for this rectangular well. The program presents them deliberately in the form of a spectrum that an experimental chemist or experimental physicist might measure. The eigenvalues correspond, of course, to the positions of the peaks. Black indicates the calculated spectrum, and purple the locations of the peaks. Notice how the peaks are broadened. During real experiments, the peaks could by broadened for a variety of reasons like the incident or target particles in the collision experiments not really being at fixed energies, or the resolutions of the detectors being large. As we mentioned before, in our case the broadening is caused by the finite time interval used for propagating the wavefunction—the longer this time interval, the less the broadening. This is a consequence of the time-energy form of Heisenberg's uncertainty principle.

For this computation, we chose the parameters input to our software differently than we did for propagation of the wavefunction. We took the starting position-space expectation value of the wavefunction to be at the center of the potential, and made the wavefunction's spread in position space small enough that it was effectively contained within the well. Recalling that only differences in potential energy are important, we set the zero point for the potential to be the bottom of the well. The "sides" of the well then corresponded to positive energies. We deliberately chose an initial kinetic energy much less than the energies of the sides, ensuring the wavefunction couldn't penetrate far into them. Such an approach ensures that the wavefunction essentially stays in the well and that there is minimal contribution from continuum eigenfunctions.

It's common in elementary quantum mechanics and quantum chemistry courses to treat the rectangular well's bound energies by solution of transcendental equations [94–99].[20] We solved these equations through bisection rootfinding. The results, along with those obtained by the three-point fit to our spectrum discussed previously are presented in Table 3. We get agreement generally to about three significant, and agreement gets better as the time step and other parameters for computation are modified to minimize error. But convergence is relatively slow as these parameters are altered, likely due to the discontinuities in the potential. For continuous potentials like the simple-harmonic oscillator's, convergence to one part in a million is readily achieved (another good exercise for modification of our source code!).[21]

[20] In advanced treatments the energies are commonly determined by examining the poles of the S-matrix [100, 101].

[21] Of course no numerical method is perfect at everything;

Table 3. Energies for the bound states for the rectangular well used here as determined by our approach, and by finding the roots of the transcendental equations specifying them.

n	E_n (**Rootfinding, energy origin at well's top**)	E_n (**Present results, energy origin at well's top**)	E_n (**Rootfinding, energy origin at well's bottom**)	E_n (**Present results, energy origin at well's bottom**)
0	$-4.745 \cdot 10^4$	$-4.749 \cdot 10^4$	$1.849 \cdot 10^3$	$1.856 \cdot 10^3$
1	$-4.199 \cdot 10^4$	$-4.196 \cdot 10^4$	$7.359 \cdot 10^3$	$7.385 \cdot 10^3$
2	$-3.295 \cdot 10^4$	$-3.289 \cdot 10^4$	$1.640 \cdot 10^4$	$1.645 \cdot 10^4$
3	$-2.069 \cdot 10^4$	$-2.063 \cdot 10^4$	$2.865 \cdot 10^4$	$2.872 \cdot 10^4$
4	$-6.214 \cdot 10^3$	$-6.172 \cdot 10^3$	$4.313 \cdot 10^4$	$4.318 \cdot 10^4$

Our eigenvalues were used by our software by the methods we described previously to generate bound-state position-space energy eigenfunctions. They are shown in Figure 6. Raw computations by our software produce results of constant, but arbitrary phase factors. Our source code automatically compensates for this, removing any imaginary part to the phases so that the eigenfunctions are provided as purely real values—which is customary. The black curves represent what our software produced. The red ones are the analytic solutions [105]. The red and black match up remarkably well, to the point where the red only "bleeds" out from the black in a few places. A glance at Figure 6 shows that our eigenfunctions have oscillatory nature inside the well, and decaying nature outside it, and are furthermore all of even or odd parity—like they must be for a symmetric well. (The decaying waves outside the well are sometimes called *evanescent*. Such waves come up often in other areas—like classical electromagnetic field theory [106, 107].) On top of this, the n^{th} eigenfunction has $n + 1$ antinodes, just like it has to [108]. A good, simple check on the validity of the results our program produces is whether the antinodes turn out this way or not.

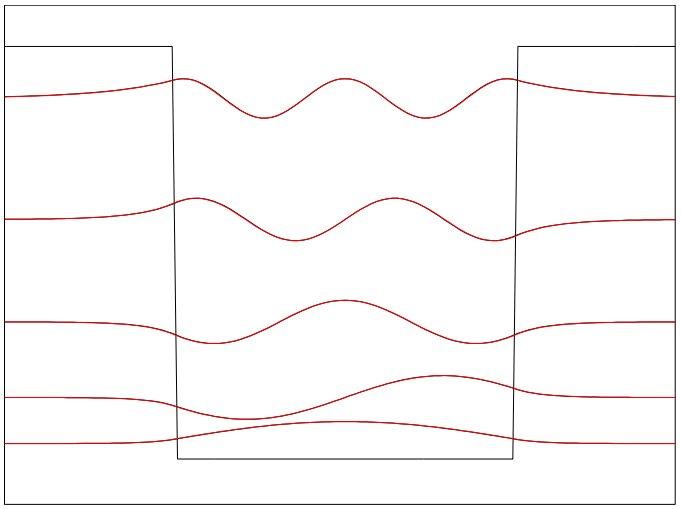

Figure 6. The rectangular well along with position-space representations of the five bound-state energy eigenfunctions whose energy eigenvalues were given in Table 3. The n^{th} of these can easily be identified by the number of nodes it has. Vertical spacings correspond to energy differences, and the wavefunctions have purely real values—as we mentioned.

3.5 Internuclear Vibrations of Diatomic Molecules

The rectangular potential we just treated was only a model—albeit a good enough one for rudimentary descriptions of systems like the deuteron in nuclear physics [109]. Next we go on to a more realistic potential—one corresponding to the interaction of atoms and how they can pair together to make diatomic molecules.

There are plenty of particles to keep track of even for fairly simple diatomic molecules—lots of electrons, and usually even more protons and neutrons stuck together in the atoms' nuclei. Fortunately the nuclei and electrons have very different masses. This means that the electrons do most of the moving around, continuously adjusting themselves in response to the much greater inertia of the nuclei. Mathematically this allows us to separate any molecular wavefunction into the product of nuclear and electronic parts to very good accuracy—the Born-Oppenheimer approximation [110].

Both nuclei making up the atoms in a diatomic molecule can move, and we simplify the motion described by their (separated) part of the wavefunction in the usual way. Let the locations

"shooting" to get eigenvalues combined with Numerov's method, for instance, is often better than the one we used here for determining eigenvalues and eigenfunctions [102–104]. But for such numerical approaches the eigenvalues have to be found one-at-a-time, with the possibility that some might be skipped over. The approach we employ here provides all the eigenvalues in one calculation.

of nuclei A and B be $\mathbf{r}_A$ and $\mathbf{r}_B$, respectively. The relative distance r between them is then just $r = |\mathbf{r}_B - \mathbf{r}_A|$. If the corresponding atomic masses are μ_A and μ_B, then their relative motion is the same as that of a single particle of reduced mass $\mu = \mu_A\mu_B/(\mu_A + \mu_B)$ [111, 112].

When atoms get close enough together they tend to attract through mutual polarization—van der Waals forces. These forces manifest themselves on the everyday scale as a correction to the ideal-gas law [113–115]. The leading potential-energy term for the van der Waals interaction goes as $1/r^6$; it's due to electric-dipole interactions. Higher-order electromagnetic multipoles contribute also, but in a diminished way[116]. As the atoms get still even closer together their electrons begin to push each other apart, exposing the almost "bare" nuclei to each other. This results in strong repulsion between the nuclei. Historically the form of this repulsion has been taken to scale as $1/r^{12}$, partly on account of the ease of calculating it by simply squaring the $1/r^6$ term [117]. The result is the Lennard-Jones potential

$$V(r) = 4\epsilon\left(\left(\frac{\sigma}{r}\right)^{12} - \left(\frac{\sigma}{r}\right)^{6}\right), \qquad (31)$$

where ϵ is the depth of the potential and σ is the distance between the nuclei where the potential changes from positive to negative [118].

Plenty of other potentials mimicking the electromagnetic-multipole interaction of atoms at short ranges have been developed. A common one—and the one we employ here—is the Morse potential [119, 120]. It has the form

$$V(r) = D\left(e^{-2a(r-r_0)} - 2e^{-a(r-r_0)}\right), \qquad (32)$$

where D is the well depth, r_0 is the average internuclear distance—the molecule's bond length—and a characterizes the potential's width. Besides its application in the treatment of diatomic molecules, this potential can also be used for situations like the lattice oscillations of atoms in crystalline solids [121].

An important advantage the Morse potential has over many of its rivals is that the time-independent part of its Schrödinger equation can be factorized into creation and destruction operators, immediately leading to an exact set of bound-state energy eigenvalues and a simple integration process to determine their corresponding position-space eigenfunctions [122–125]. For the former we get

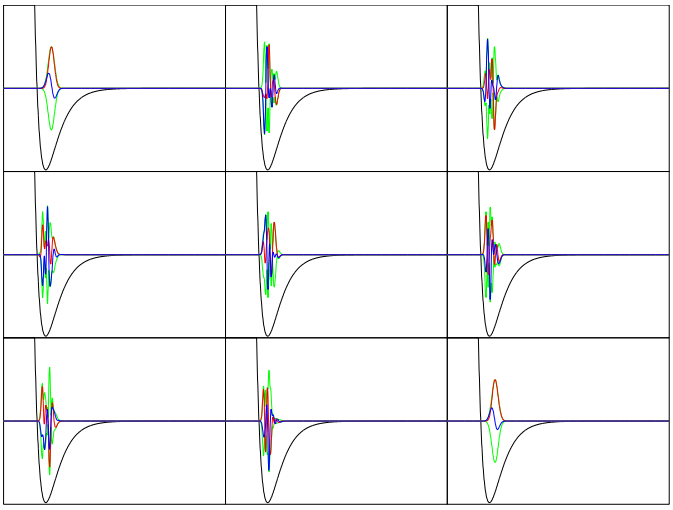

Figure 7. Internuclear vibrations for molecular oxygen. The horizontal axis corresponds to internuclear separation, while along the vertical axis are the potential and the real part, imaginary part, and modulus of the wavefunction. The time values were 0, 5000, 10000, 30000, 50000, 80000, 100000, 130000 and 169163.

$$E_\nu = a\hbar\sqrt{\frac{2D}{\mu}}\left(\nu + \frac{1}{2}\right) - \frac{a^2\hbar^2}{2\mu}\left(\nu + \frac{1}{2}\right)^2, \qquad (33)$$

where the quantum number ν goes from 0 to some maximum value that depends on D and a.

To explore the Morse potential with our source code we made calculations for the nuclear part of the wavefunction going with the ground electronic $X^3\Sigma_g^-$ state of molecular oxygen (O_2) using parameters characterizing it that were established decades ago [126–129].[22] Our propagation results are shown in Figure 7. Instead of giving the probability density—as we did previously—we displayed the wavefunction itself. (Our source code contains a "switch" to easily change between these two display modes.) The green curves are the positive and negative moduli or "absolute values" of the wavefunction. They act as envelopes for its real and imaginary parts which are shown in blue and red, respectively. The black curve is the potential.

For these calculations we chose a range in position space of 12, a spread in the initial wavefunction $\sigma = 1\%$ this range, and an initial position of the bond length plus 3. The initial wavenumber was 3, and

[22] The ground, or "X," electronic states of most diatomic molecules are completely symmetric: $^1\Sigma$. The spin-triplet character of O_2's X state is therefore kind of unusual [130]. Another common diatomic molecule which is unusual in this way is nitric oxide (NO); NO's X state has $^2\Pi$ symmetry [131, 132].

a time step of 1 was used over $2^{18} = 262144$ saved steps. Each saved step was split into 9 hidden steps according to Eqn. 13. The size of the array containing the wavefunction was $2^{10} = 1024$, and the mass used was the reduced mass of molecular oxygen.

The wavefunction in Figure 7 starts out with fairly simple real and imaginary parts. But over its evolution these parts—along with the wavefunction's modulus—get quite complicated. They exhibit multiple maxima and minima which emerge and disappear while moving from place to place throughout the frames. Then in the last frame the wavefunction returns pretty close to its form in the first frame; a comparison of the wavefunctions in these frames using Eqn. 14 shows that they are more than 99% the same as each other.

This suggests repetition, and repetition is *almost* what's happening here. All *bound* systems—whether classical or quantum-mechanical—come arbitrarily close to repeating themselves, even though the period could amount to a very, very long time. This "recurrence" is a little more transparent in quantum mechanics than in classical mechanics [133–137].

3.6 Determination of Bound-State Energy Eigenvalues and Position-Space Energy Eigenfunctions for the Morse Potential

The spectrum resulting from our propagation is given in Figure 8. There are 50 peaks, each one corresponding to a bound state supported by the potential well. The black curve is the calculated energy spectrum, while the purple lines are the locations of the eigenvalues. Note how much narrower the peaks are compared to those we got for the rectangular well. This is due to the much longer propagation time for the wavefunction. Table 4 lists values for several of the peaks, along with values determined from Eqn. 33. Agreement among the numbers is quite reasonable.

Figure 9 shows the position-space bound-state eigenfunctions our software calculated for the

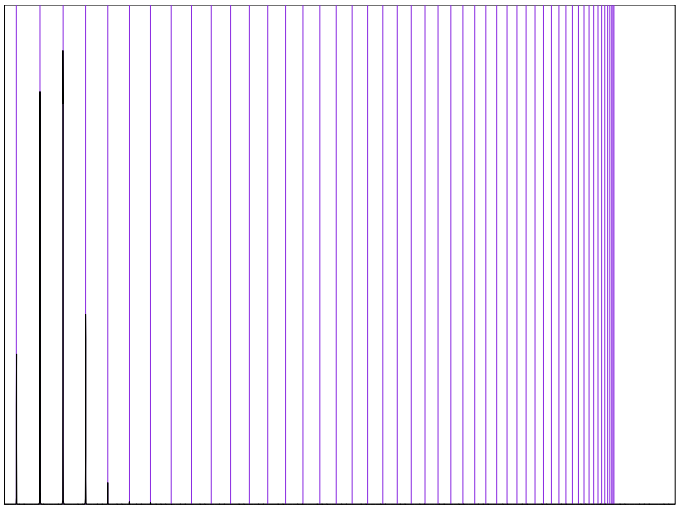

Figure 8. Energy spectrum for the Morse potential of the ground electronic state of molecular oxygen. Some of the peaks are bunched up too closely to be seen distinctly.

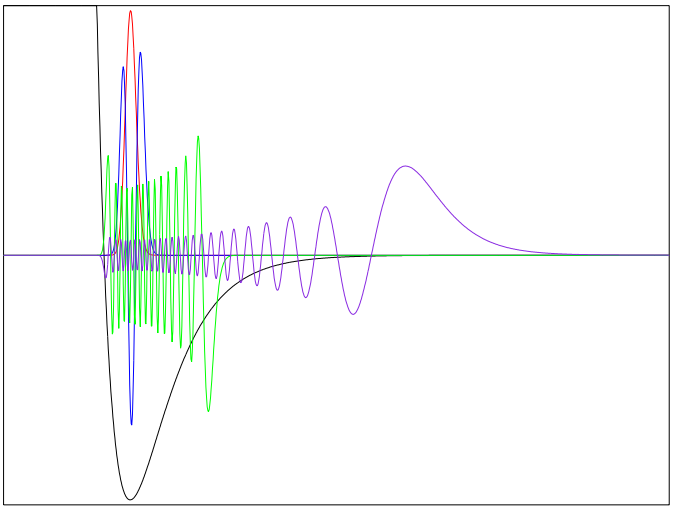

Figure 9. Selected bound-state position-space energy eigenfunctions of the Morse potential for molecular oxygen.

eigenvalues in Table 4. The red one is for $\nu = 0$. It has a single anti-node centered on the equilibrium internuclear distance of molecular oxygen—O_2's bond length. The eigenfunction for $\nu = 2$ is shown in blue, that for $\nu = 27$ in green, and the one for $\nu = 49$ in purple. As the value of ν goes up, the maximum

Table 4. Energies for selected bound states of the Morse potential.

ν	E_ν (**Analytic, energy origin at well's top**)	E_ν (**Present results, energy origin at well's top**)	E_ν (**Analytic, energy origin at well's bottom**)	E_ν (**Present results, energy origin at well's bottom**)
0	$3.751 \cdot 10^{-3}$	$3.754 \cdot 10^{-3}$	$-1.878 \cdot 10^{-1}$	$-1.878 \cdot 10^{-1}$
2	$1.114 \cdot 10^{-2}$	$1.115 \cdot 10^{-2}$	$-1.804 \cdot 10^{-1}$	$-1.803 \cdot 10^{-1}$
27	$1.512 \cdot 10^{-1}$	$1.512 \cdot 10^{-1}$	$-4.029 \cdot 10^{-2}$	$-4.030 \cdot 10^{-2}$
49	$1.914 \cdot 10^{-1}$	$1.914 \cdot 10^{-1}$	$-1.260 \cdot 10^{-4}$	$-1.507 \cdot 10^{-4}$

modulus of the eigenfunction moves farther and farther beyond the bond length, to the point that the oxygen molecule is almost dissociated into two separate oxygen atoms—just like we expect.

4 Conclusion

To enhance the instruction and learning of quantum mechanics and quantum chemistry we have developed Fortran source code to solve Schrödinger's equation in one spatial dimension, and to display the consequent evolving wavefunctions in real time as movies or as single frames from these movies, depending on the user's wishes. In addition to propagating wavefunctions the source code can determine bound-state energy eigenvalues and their corresponding position-space eigenfunctions.

Rather than harboring on the details of the source code, we emphasized the physics, chemistry, mathematics, and numerical algorithms that underlie it. We provided plenty of citations and footnotes to give historical perspective on the parts of quantum mechanics and quantum chemistry relevant to what we did here, and to enable others to modify and extend the source code for their own projects. The source code can be freely downloaded for non-commercial, educational purposes, like we already said.

Our source code has been tested and to the best of our knowledge has no flaws. Nonetheless, we make no warranties, implied or expressed, that the source code is free of error. It should not be used for any purpose in which incorrect results that it might produce could result in personal injury, loss of life, property damage, or property loss. All use of the source code, including modified versions of it, is at the user's own risk. We disclaim all liability for direct or consequential damage resulting from use of this source code or anything derived from it or its modifications. With all that said, feel free to download the source code, modify it as needed, and have some fun with it for your own projects!

Data Availability Statement

The data and source code supporting the findings of this study are publicly available in the GitHub repository: https://github.com/cjssjccjs/qmechonedim/.

Funding

This work was supported without any funding.

Conflicts of Interest

The authors declare no conflicts of interest.

AI Use Statement

The authors declare that no generative AI was used in the preparation of this manuscript.

Ethical Approval and Consent to Participate

Not applicable.

References

[1] Heisenberg, W. (1925). Über quantentheoretische Umdeutung kinematischer und mechanischer Beziehungen. *Zeitschrift für Physik, 33*(1), 879-893. [CrossRef]

[2] Born, M., & Jordan, P. (1925). Zur quantenmechanik. *Zeitschrift für Physik, 34*(1), 858-888. [CrossRef]

[3] Born, M., Heisenberg, W., & Jordan, P. (1926). Zur quantenmechanik. II. *Zeitschrift für Physik, 35*(8), 557-615. [CrossRef]

[4] Dirac, P. A. M. (1925). The fundamental equations of quantum mechanics. *Proceedings of the Royal Society of London. Series A, Containing Papers of a Mathematical and Physical Character, 109*(752), 642-653. [CrossRef]

[5] Dirac, P. A. M. (1927). The physical interpretation of the quantum dynamics. *Proceedings of the Royal Society of London. Series A, Containing Papers of a Mathematical and Physical Character, 113*(765), 621-641. [CrossRef]

[6] Feynman, R. P. (1948). Space-time approach to non-relativistic quantum mechanics. *Reviews of Modern Physics, 20*(2), 367-387. [CrossRef]

[7] Feynman, R. P., & Hibbs, A. R. (2010). *Quantum Mechanics and Path Integrals*. Dover Publications.

[8] Schrödinger, E. (1926). Quantisierung als Eigenwertproblem. *Annalen der Physik* (*Leipzig*), 79, 361-76. [CrossRef]

[9] Schrödinger, E. (1926). Quantisierung als Eigenwertproblem. *Annalen der Physik* (*Leipzig*), 79, 489-527. [CrossRef]

[10] Schrödinger, E. (1926). Über das Verhältnis der Heisenberg-Born-Jordanshen Quantenmechanik zu der meinen. *Annalen der Physik* (*Leipzig*), 79, 734-56. [CrossRef]

[11] Schrödinger, E. (1926). Quantisierung als Eigenwertproblem. *Annalen der Physik* (*Leipzig*), 80, 437-90. [CrossRef]

[12] Schrödinger, E. (1926). Quantisierung als Eigenwertproblem. *Annalen der Physik* (*Leipzig*), 81, 109-39. [CrossRef]

[13] Eckart, C. (1926). Operator calculus and the solution

of the equations of quantum dynamics. *Physical Review, 28*(4), 711-26. [CrossRef]

[14] Landau, L. D., & Lifshitz, E. M. (1977) *Quantum Mechanics* (*Non-relativistic Theory*). Pergamon Press. https://power1.pc.uec.ac.jp/~toru/notes/LandauLifshitz-QuantumMechanics.pdf

[15] Pauling, L., & Wilson, E. B. (1985). *Introduction to Quantum Mechanics: with applications to chemistry*. Courier Corporation.

[16] Blatt, J. M., & Weisskopf, V. F. (2012). *Theoretical Nuclear Physics*. Springer Science & Business Media.

[17] Newton, R. G. (2013). *Scattering Theory of Waves and Particles*. Springer Science & Business Media.

[18] Taylor, J. R. (2012). *Scattering theory: the Quantum Theory of Nonrelativistic Collisions*. Courier Corporation.

[19] Fleck Jr, J. A., Morris, J. R., & Feit, M. D. (1976). Time-dependent propagation of high energy laser beams through the atmosphere. *Applied physics, 10*(2), 129-160. [CrossRef]

[20] Feit, M. D., Fleck Jr, J. A., & Steiger, A. (1982). Solution of the Schrödinger equation by a spectral method. *Journal of Computational Physics, 47*(3), 412-433. [CrossRef]

[21] Feit, M. D., & Fleck Jr, J. A. (1983). Solution of the Schrödinger equation by a spectral method II: Vibrational energy levels of triatomic molecules. *The Journal of Chemical Physics, 78*(1), 301-308. [CrossRef]

[22] Feit, M. D., & Fleck Jr, J. A. (1984). Wave packet dynamics and chaos in the Hénon–Heiles system. *The Journal of Chemical Physics, 80*(6), 2578-2584. [CrossRef]

[23] Sweeney, C. J., & De Vries, P. L. (1989). Time-dependent quantum-mechanical scattering in two dimensions. *Computers in Physics, 3*(1), 49-54. [CrossRef]

[24] Dyson, F. J. (1949). The radiation theories of Tomonaga, Schwinger, and Feynman. *Physical Review, 75*(3), 486. [CrossRef]

[25] Bandrauk, A. D., & Shen, H. (1992). Higher order exponential split operator method for solving time-dependent Schrödinger equations. *Canadian Journal of Chemistry, 70*(2), 555-559. [CrossRef]

[26] Sakurai, J. J., & Napolitano, J. (2020). *Modern quantum mechanics*. Cambridge university press.

[27] Hardin, R. H. (1973). Application of the split-step Fourier method to the numerical solution of nonlinear and variable coefficient wave equations. *SIAM Rev., 15*, 423.

[28] Baker, H. F. (1904). On functions of several variables. *Proceedings of the London Mathematical Society, 2*(1), 14-36. [CrossRef]

[29] Campbell, J. E. (1897). On a law of combination of operators (second paper). *Proceedings of the London Mathematical Society, 1*(1), 14-32. [CrossRef]

[30] Hausdorff, F. (1906). Die symbolische Exponentialformel in der Gruppentheorie. *Ber. Verh. Kgl. SÃ¤chs. Ges. Wiss. Leipzig., Math.-phys. Kl., 58*, 19-48. https://cds.cern.ch/record/435181

[31] Trotter, H. F. (1959). On the product of semi-groups of operators. *Proceedings of the American Mathematical Society, 10*(4), 545-551. [CrossRef]

[32] Wilcox, R. M. (1967). Exponential operators and parameter differentiation in quantum physics. *Journal of Mathematical Physics, 8*(4), 962-982. [CrossRef]

[33] Veltman, M. (1994). *Diagrammatica: the path to Feynman diagrams* (No. 4). Cambridge University Press.

[34] Tannor, D. (2008). *Introduction to quantum mechanics: a time-dependent perspective*. MIT Press.

[35] Ruth, R. D. (2007). A Canonical Integration Technique. *IEEE Transactions on Nuclear Science, 30*(4), 2669-2671. [CrossRef]

[36] Hatano, N., & Suzuki, M. (2005). Finding exponential product formulas of higher orders. In *Quantum annealing and other optimization methods* (pp. 37-68). Berlin, Heidelberg: Springer Berlin Heidelberg. [CrossRef]

[37] Burden, R. L., Faires, J. D., & Burden, A. M. (2016). *Numerical Analysis* (10th ed.). Cengage Learning.

[38] Ziman, J. M. (1972). *Principles of the Theory of Solids* (2nd ed.). Cambridge University Press.

[39] Kittel, C., & Fong, C. Y. (1963). *Quantum theory of solids* (2nd ed.). New York: Wiley. [CrossRef]

[40] Churchill, R. V. (1972). *Operational Mathematics* (3rd ed.). McGraw-Hill.

[41] DeVries, P. L., & Hasbun, J. E. (2011). *A First Course in Computational Physics* (2nd ed.). Jones and Bartlett.

[42] Schiff, L. I. (1968). *Quantum Mechanics* (3rd ed.). McGraw-Hill.

[43] von Neumann, J. (2055). Mathematical Foundations of Quantum Mechanics: Princeton Univ. Press. [CrossRef]

[44] Baym, G. (1990). *Lectures on Quantum Mechanics*. Westview Press.

[45] Merzbacher, E. (1998). *Quantum Mechanics* (3rd ed.). John Wiley & Sons.

[46] Gottfried, K., & Yan, T. M. (2013). *Quantum Mechanics: Fundamentals*. Springer Science & Business Media.

[47] Jackson, J. D. (2006). *Mathematics for quantum mechanics: an introductory survey of operators, eigenvalues, and linear vector spaces*. Courier Corporation.

[48] Franklin, P. (1968). *A Treatise on Advanced Calculus*. Dover Publications.

[49] Bartle, R. G. (1976). *The Elements of Real Analysis* (2nd ed.). John Wiley & Sons.

[50] Halperin, I., & Schwartz, L. (1952). *Introduction to the Theory of Distributions*. University of Toronto Press.

[CrossRef]

[51] Butkov, E. (1968). *Mathematical Physics*. Addison-Wesley Publishing Company.

[52] Hylleraas, E. A. (1970). *Mathematical and Theoretical Physics* (2 vols.). John Wiley & Sons. https://archive.org/details/mathematicaltheo0001hyll

[53] Dirac, P. A. M. (1981). *The principles of quantum mechanics* (No. 27). Oxford university press.

[54] Balakrishnan, V. (2003). All about the Dirac delta function (?). *Resonance, 8*(8), 48-58. [CrossRef]

[55] Harris, F. J. (1978). On the use of windows for harmonic analysis with the discrete Fourier transform. *Proceedings of the IEEE, 66*(1), 51-83. [CrossRef]

[56] Bevington, P. R., & Robinson, D. K. (2003). *Data reduction and error analysis* (Vol. 3). New York: McGraw-Hill. http://www.spy-hill.net/myers/vassar/201/notes/textalk.pdf

[57] Pang, T. (2006). *An Introduction to Computational Physics* (2nd ed.). Cambridge University Press.

[58] Feit, M. D., & Fleck Jr, J. A. (1980). Computation of mode properties in optical fiber waveguides by a propagating beam method. *Applied Optics, 19*(7), 1154-1164. [CrossRef]

[59] Swokowski, E. W. (1983). *Calculus with Analytic Geometry* (alt. ed.). Prindle, Weber & Schmidt.

[60] Zill, D. G. (1982). *A First Course in Differential Equations with Applications* (9th ed.). Prindle, Weber & Schmidt. https://ilkomitt.wordpress.com/wp-content/uploads/2016/01/dennis-g-zill_a-first-course-in-differential-equations-9th-ed.pdf

[61] Griffiths, D. J., & Schroeter, D. F. (2018). *Introduction to quantum mechanics*. Cambridge university press.

[62] Hamermesh, M. (1989). *Group Theory and its Application to Physical Problems*. Dover Publications.

[63] Tinkham, M. (2003). *Group theory and quantum mechanics*. Courier Corporation.

[64] Schatz, G. C., & Ratner, M. A. (2002). *Quantum mechanics in chemistry*.

[65] Pauli Jr, W. (1926). Über das Wasserstoffspektrum vom Standpunkt der neuen Quantenmechanik. *Zeitschrift für Physik A Hadrons and NAuclei, 36*(5), 336-363. [CrossRef]

[66] McIntosh, H. V. (1959). On accidental degeneracy in classical and quantum mechanics. *American Journal of Physics, 27*(9), 620-625. [CrossRef]

[67] Gauss, C. F. (1866). Nachlass: Theoria interpolationis methodo nova tractata. *Carl Friedrich Gauss Werke, 3*, 265-327. https://archive.org/details/werkecarlf03gausrich

[68] Danielson, G. C., & Lanczos, C. (1942). Some improvements in practical Fourier analysis and their application to X-ray scattering from liquids. *Journal of the Franklin Institute, 233*(5), 435-452. [CrossRef]

[69] Cooley, J. W., & Tukey, J. W. (1965). An algorithm for the machine calculation of complex Fourier series. *Mathematics of computation, 19*(90), 297-301. [CrossRef]

[70] Brigham, E. O. (1974). *The Fast Fourier Transform*. Prentice-Hall. https://archive.org/details/fastfouriertrans00brig

[71] Zonst, A. E. (2000). *Understanding the FFT: A Tutorial on the Algorithm & Software for Laymen, Students, Technicians & Working Engineers* (2nd rev. ed.). Citrus Press. https://archive.org/details/understandingfft0000zons

[72] Wyld, H. W. (1976). *Mathematical Methods for Physics*. W. A. Benjamin. https://inis.iaea.org/records/3q91n-bbn69

[73] Churchill, R. V., & Brown, J. W. (1984). *Complex Variables and Applications* (4th ed.). McGraw-Hill. https://archive.org/details/complexvariables0000jame/page/n1/mode/2up

[74] Nyquist, H. (1928). Certain topics in telegraph transmission theory. *Transactions of the American Institute of Electrical Engineers, 47*(2), 617-644. [CrossRef]

[75] Shannon, C. (1949). Communication in the Presence of Noise. *Proceedings of the Institute of Radio Engineers*, 37, 10-21. [CrossRef]

[76] Andrews, L. C., & Shivamoggi, B. K. (1988). *Integral Transforms for Engineers and Applied Mathematicians*. Macmillan. https://archive.org/details/integraltransfor0000andr_g3t2

[77] Landau, L. D., & Lifshitz, E. M. (1976). *Mechanics* (3rd ed.). Elsevier Butterworth-Heinemann. https://www.abebooks.com/COURSE-THEORETICAL-PHYSICS-VOLUME-MECHANICS-3ED/32436853333/bd

[78] Nuttall, A. H. (1981). Some Windows with Very Good Sidelobe Behavior. *IEEE Transactions on Acoustics, Speech, and Signal Processing*, 29, 84-91. [CrossRef]

[79] Press, W. H., Teukolsky, S. A., Vetterling, W. T., & Flannery, B. P. (1997). *Numerical Recipes in Fortran 90: The Art of Parallel Scientific Computing* (2nd ed., 2 vols.). Cambridge University Press. https://archive.org/details/numericalrecipes0000unse_k9a7

[80] Backus, J. (1998). The History of Fortran I, II, and III. *IEEE Annals of the History of Computing, 20*, 68-78. [CrossRef]

[81] Krill, P. (2024, May 6). *Fortran popularity rises with numerical and scientific computing*. InfoWorld. Retrieved from https://www.infoworld.com/article/2337114/fortran-popularity-rises-with-numerical-and-scientific-computing.html

[82] Hartree, D. R. (1928, January). The wave mechanics of an atom with a non-Coulomb central field. Part I. Theory and methods. In *Mathematical Proceedings of the Cambridge Philosophical Society, 24*(1), 89-110. Cambridge university press. [CrossRef]

[83] McWeeney, R. (1973). Natural Units in Atomic and Molecular Physics. *Nature, 243*(5), 196-198.

[CrossRef]

[84] Liboff, R. I. (2003). *Introductory Quantum Mechanics* (4th ed.). Addison-Wesley. https://dn790006.ca.archive.org/0/items/LIBOFFIntroductoryQuantumMechanics/LIBOFF%20-%20Introductory%20Quantum%20Mechanics.pdf

[85] Goldberg, A., Schey, H. M., & Schwartz, J. L. (1967). Computer-generated motion pictures of one-dimensional quantum-mechanical transmission and reflection phenomena. *American Journal of Physics, 35*(3), 177-186. [CrossRef]

[86] McMurray, J., & Fay, R. C. (2001). *Chemistry* (3rd ed.). Prentice-Hall. [CrossRef]

[87] Knight, R. D. (2013). *Physics for Scientists and Engineers with Modern Physics* (3rd ed.). Pearson Education.

[88] Schulz, G. J. (1973). Resonances in electron impact on diatomic molecules. *Reviews of Modern Physics, 45*(3), 378-486. [CrossRef]

[89] Biondi, M. A., Herzenberg, A., & Kuyatt, C. E. (1979). Resonances in atoms and molecules. *Physics Today, 32*(10), 44-49. [CrossRef]

[90] Wu, T. Y., & Ohmura, T. (2014). *Quantum theory of scattering*. Courier Corporation.

[91] Kane, G. (1993). *Modern elementary particle physics*. Cambridge Univ. Press. https://www.cambridge.org/us/universitypress/subjects/physics/particle-physics-and-nuclear-physics/modern-elementary-particle-physics-explaining-and-extending-standard-model-2nd-edition

[92] Arfken, G. B., Weber, H. J., & Harris, F. E. (2011). *Mathematical methods for physicists: a comprehensive guide*. Academic Press. [CrossRef]

[93] Brown, J. W., & Churchill, R. V. (2015). *Fourier Series and Boundary Value Problems* (8th ed.). McGraw-Hill Education Private Limited.

[94] Pitkanen, P. H. (1955). Rectangular potential well problem in quantum mechanics. *American Journal of Physics, 23*(2), 111-113. [CrossRef]

[95] Guest, P. (1972). Graphical solutions for the square well. *American Journal of Physics, 40*, 1175-1176. [CrossRef]

[96] Saxon, D. S. (2013). *Elementary Quantum Mechanics*. Dover Publications.

[97] de Alcantara Bonfim, O. F., & Griffiths, D. J. (2006). Exact and approximate energy spectrum for the finite square well and related potentials. *American journal of physics, 74*(1), 43-48. [CrossRef]

[98] Sternberg, S. (2019). *A Mathematical Companion to Quantum Mechanics*. Dover Publications.

[99] Reed, B. C. (2021). A guide to the literature of the finite rectangular well. *American Journal of Physics, 89*(5), 529-534. [CrossRef]

[100] Mott, H. F., & Massey, H. S. W. (1965). *The Theory of Atomic Collisions* (3rd ed.). Oxford University Press.

[101] Roman, P. (1965). *Advanced Quantum Theory: An Outline of the Fundamental Ideas*. Addison-Wesley. https://archive.org/details/advancedquantumt0000roma

[102] Noumerov, B. V. (1924). A method of extrapolation of perturbations. *Monthly Notices of the Royal Astronomical Society, 84*(6), 592-602. [CrossRef]

[103] Numerov, B. (1927). Note on the numerical integration of d2x/dt2= f (xt). *Astronomische Nachrichten, 230*(19), 359-364. [CrossRef]

[104] Koonin, S. E. (2018). *Computational physics: Fortran version*. CRC Press. https://archive.org/details/computationalphy0000koon

[105] Yariv, A. (1982). *An Introduction to Theory and Applications of Quantum Mechanics*. Dover Publications.

[106] Frankl, D. R. (1986). *Electromagnetic Theory*. Prentice-Hall.

[107] Jackson, J. D. (1999). *Classical Electrodynamics* (3rd ed.). John Wiley & Sons. [CrossRef]

[108] Messiah, A. (2014). *Quantum mechanics*. Courier Corporation.

[109] McTavish, J. P. (1982). Separable potentials and their momentum-energy dependence. *Journal of Physics G: Nuclear Physics, 8*(8), 1037-1048. [CrossRef]

[110] Born, M., & Oppenheimer, R. (1927). Zur quantentheorie der molekeln. *Annalen der Physik (Leipzig), 389*(20), 457-484. [CrossRef]

[111] Fowles, G. R. (1986). *Analytical Mechanics* (4th ed.). Saunders College Publishing. https://archive.org/details/analyticalmechan0000fowl_h7b9

[112] Goldstein, H., Poole, C., & Safko, J. (2002). *Classical Mechanics* (3rd ed.). Addison-Wesley. https://archive.org/details/HerbertGoldsteinCharlesPooleJohnSafkoClassicalMechanics3rdEd/page/n5/mode/2up

[113] Uhlenbeck, G. E., Ford, G. W., & Montroll, E. W. (1963). *Lectures in Statistical Mechanics*. American Mathematical Society. https://digitalcommons.rockefeller.edu/ru-authors/168/

[114] Sears, F. W., & Salinger, G. L. (1975). *Thermodynamics, Kinetic Theory, and Statistical Thermodynamics (3rd ed.)*. Addison-Wesley. https://archive.org/details/thermodynamicski0000sear

[115] Huang, K. (1987). *Statistical Mechanics* (3rd ed.). John Wiley & Sons.

[116] Cohen-Tannoudji, C., Diu, B., & Laloë, F. (1977). *Quantum Mechanics* (2 vols.). John Wiley & Sons. https://www.wiley.com/en-us/Quantum+Mechanics%2C+Volume+1%3A+Basic+Concepts%2C+Tools%2C+and+Applications%2C+2nd+Edition-p-9783527822713

[117] Lenhard, J., Stephan, S., & Hasse, H. (2024). On the History of the Lennard-Jones Potential. *Annalen der Physik (Leipzig), 536*(6), 2400115. [CrossRef]

[118] Levine, I. R. (2017). *Quantum Chemistry* (7th ed.). Pearson India Education Services Pvt. Ltd. http://macl-ustm.digitallibrary.co.in/handle/123456789/3252

[119] Morse, P. M. (1929). Diatomic molecules according to the wave mechanics. II. Vibrational levels. *Physical review, 34*(1), 57-64. [CrossRef]

[120] Pekeris, C. L. (1934). The Rotation-Vibration Coupling in Diatomic Molecules. *Physical Review, 45*(4), 98-103. [CrossRef]

[121] Girifalco, L. A., & Weizer, V. G. (1959). Application of the Morse potential function to cubic metals. *Physical Review, 114*(3), 687-690. [CrossRef]

[122] Schrödinger, E. (1940, January). A method of determining quantum-mechanical eigenvalues and eigenfunctions. In *Proceedings of the Royal Irish Academy. Section A: Mathematical and Physical Sciences, 46*(1), 9-16. https://www.jstor.org/stable/20490744

[123] Infeld, L., & Hull, T. E. (1951). The factorization method. *Reviews of modern Physics, 23*(1), 21-68. [CrossRef]

[124] Dong, S. H., Lemus, R., & Frank, A. (2002). Ladder operators for the Morse potential. *International Journal of Quantum Chemistry, 86*(5), 433-439. [CrossRef]

[125] Hecht, K. T. (2012). *Quantum mechanics*. Springer Science & Business Media.

[126] Konowalow, D. D., & Hirschfelder, J. O. (1961). Morse Potential Parameters for O–O, N–N, and N–O Interactions. *The Physics of Fluids, 4*(5), 637-642. [CrossRef]

[127] Rosen, B. (Ed.). (1970). *Constantes Sélectionnées Données Spectroscopiques relatives aux Molécules Diatomiques*. Pergamon Press. https://search.worldcat.org/title/2187305

[128] Huber, K. P., & Herzberg, G. (1979). *Molecular Spectra and Molecular Structure IV. Constants of Diatomic Molecules*. Van Nostrand Reinhold. [CrossRef]

[129] Shyn, T. W., & Sweeney, C. J. (1993). Vibrational-excitation cross sections of molecular oxygen by electron impact. *Physical Review A, 48*(2), 1214-1217. [CrossRef]

[130] Vemulapalli, G. K. (1993). *Physical Chemistry*. Prentice-Hall. https://archive.org/details/physicalchemistr0000vemu

[131] King, G. W. (1964). *Spectroscopy and Molecular Structure*. Holt, Rinehart, and Winston. https://www.semanticscholar.org/paper/Spectroscopy-and-Molecular-Structure-King/2ccbb5258bdbb14e9296c9130869cce98b4867c6

[132] Pilar, F. L. (2001). *Elementary Quantum Chemistry* (2nd ed.). Dover Publications.

[133] Poincaré, H. (1890). Sur le problème des trois corps et les équations de la dynamique. *Acta Mathematica, 13*(1), 1-270. [CrossRef]

[134] Bocchieri, P., & Loinger, A. (1957). Quantum Recurrence Theorem. *Physical Review, 107*(102), 337-8. [CrossRef]

[135] Percival, I. C. (1961). Almost periodicity and the quantal H theorem. *Journal of Mathematical Physics, 2*(2), 235-239. [CrossRef]

[136] Schulman, L. S. (1978). Note on the quantum recurrence theorem. *Physical Review A, 18*(5), 2379-2380. [CrossRef]

[137] Sewell, G. L. (2014). *Quantum theory of collective phenomena*. Courier Corporation.

Christopher J. Sweeney earned a B.S. degree in physics from Miami University (Ohio) and both M.S. and Ph.D. degrees in physics from the University of Michigan (Ann Arbor). Currently a physics professor, he spent more than a decade as a professional researcher in experimental atomic physics and rocket science. Here he is shown working on the scientific instruments for a NASA sounding rocket mission to investigate the possibility that the planet Venus may have had oceans of liquid water on it billions of years ago, even though it's bone-dry right now. (Email: sweeneyc@nwfsc.edu)